DOI: 10.61782/fa.2025.0812

FORUM ACUSTICUM EURONOISE 2025

SPATIAL PSYCHOACOUSTIC ANALYSIS OF PERCEPTUAL ERROR SHAPING IN LOCAL ACTIVE NOISE CONTROL

Christian Blöcher[1*] **Alois Sontacchi**[1] **Thomas Hatheier**[2]
[1] Institute of Electronic Music and Acoustics, University of Music and Performing Arts Graz, Austria
[2] Audio Mobil Elektronik GmbH, Braunau–Ranshofen, Austria

ABSTRACT

To address the frequency-dependent nature of human auditory perception, error shaping can be incorporated into traditional feedforward Filtered-Reference Least-Mean-Squares (FxLMS) local Active Noise Control (ANC) schemes by applying A-weighting to the LMS input signals. Several publications have compared the psychoacoustic properties of noise residuals produced by such Filtered-Error LMS (FeLMS) and FxLMS ANC systems at the point of cancellation. This paper expands previous studies by additionally investigating the surrounding sound field. In a co-simulation, both algorithms are evaluated for fullband and bandlimited control for an active headrest system with two built-in loudspeakers and a head and torso simulator (HATS) positioned in front of the headrest. With white, pink, and real-world driving noise as innovation signals, the sound field after adaptation is evaluated for HATS rotations and transitions to the front, utilizing psychoacoustic- and speech metrics. While the FeLMS algorithm generally produces more coloration for head movements from the reference position than the FxLMS algorithm, performance for synthetic signals is otherwise similar. However, for driving noise, it achieves greater loudness reduction and improved speech intelligibility. The spatial extent of noise control is enlarged for bandlimited compared to fullband ANC systems at the cost of reduced performance near the reference position.

Keywords: *Active Noise Control, Psychoacoustics, Speech Intelligibility.*

**Corresponding author: bloecher@iem.at.*

1. INTRODUCTION

Active Noise Control (ANC) aims at reducing unwanted noise by superimposing a destructively interfering anti-noise played via loudspeakers. The optimization goal of traditional feedforward ANC schemes relying on the Filtered-Reference Least-Mean-Squares (FxLMS) approach is the minimization of the error signal energy [1]. This corresponds to a maximization of the mean noise reduction across the entire controlled frequency spectrum. However, since this criterion ignores the frequency-dependent nature of human auditory perception [2], the achieved noise reduction may be suboptimal. A simple, yet effective way of incorporating the frequency characteristic of our hearing system is perceptual error shaping. In a Filtered-Error LMS (FeLMS) ANC approach [3], a psychoacoustic rating filter, such as A-weighting, can be applied to the LMS input signals to guide the focus of the adaptation towards frequency regions in which our hearing is more sensitive [4]. Previous publications have compared the psychoacoustic properties of noise residuals produced by perceptually motivated FeLMS ANC approaches and FxLMS systems at the point of cancellation [5] or for headphone applications [6]. This paper extends the evaluation by additionally investigating the psychoacoustic properties of the surrounding sound field. In a co-simulation, both FxLMS and FeLMS algorithms are evaluated for fullband and bandlimited local control in an active headrest system for use in vehicles, utilizing both synthetic and real-world innovation signals.

The rest of this paper is organized as follows. Section 2 details the co-simulation by describing the physical measurement setup, specifying the utilized innovation signals, and highlighting the investigated ANC algorithms and adaptation procedure. Section 3 features the metrics used in the spatial psychoacoustic evaluation, before results are presented in section 4. To conclude, section 5 summarizes the findings and provides an outlook.

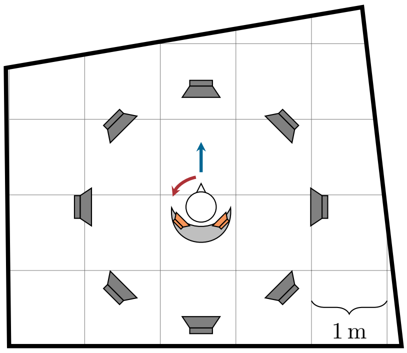

Figure 1. Measurement setup in an anechoic room with primary loudspeakers (grey), and HATS positioned in front of an active headrest with integrated secondary loudspeakers (orange). Arrows indicate directions of HATS rotation (red) and transition (blue).

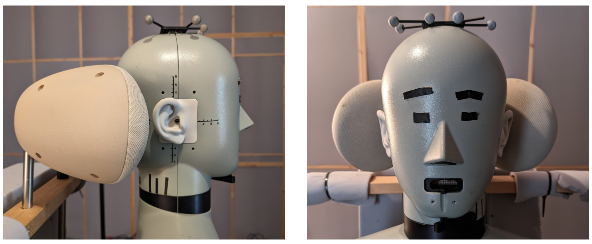

(a) Side view (b) Front view

Figure 2. Placement of the HATS in front of the headrest at the reference position.

2. CO-SIMULATION

2.1 Measurement Setup

The evaluation took place within a co-simulation based on the physical setup depicted in Fig. 1, extending the approach described in [7]. In an anechoic room, a Brüel & Kjær 4128C HATS was positioned in front of an active headrest situated in the center of a circular arrangement of eight Genelec 8020B loudspeakers with a radius of $1.45\,\mathrm{m}$. While these loudspeakers served as the primary sources, two loudspeakers integrated into the headrest in close proximity to the HATS' ears were utilized as secondary sources. To model this scenario within the co-simulation, both the acoustic primary paths between the loudspeakers in the circular arrangement and the HATS, and the acoustic secondary paths between the headrest loudspeakers and the HATS were measured at a sample rate of $44.1\,\mathrm{kHz}$ using the method of multiple exponential sine sweeps [8]. Starting from the neutral HATS position shown in Fig. 2 as a reference position, the measurement procedure was repeated for rotations of the HATS of up to $30°$ to the left in $1°$ steps and lateral transitions of the HATS of up to $15\,\mathrm{cm}$ to the front in $0.5\,\mathrm{cm}$ steps. To ensure the accuracy of the re-positioning of the HATS, rotations were executed using a motorized turntable and the HATS' position was verified using an optical tracking system (OptiTrack Motive with 6 Flex3 cameras, mean error $\leq 0.5\,\mathrm{mm}$) for both rotations and transitions.

2.2 Innovation Signals

For the co-simulation, both synthetic and real-world innovation signals were utilized. As synthetic test signals, $75\,\mathrm{s}$ of mono white and pink noise were generated at a sample rate of $44.1\,\mathrm{kHz}$. Additionally, a recording of driving noise captured using an NTi MA2230 measurement microphone in a car (combustion engine, $80\,\mathrm{km/h}$) was cut to the same duration. To achieve a diffuse presentation, all innovation signals were processed using the IEM Plugin Suite's [1] Granular Encoder [9] as described by Holzmüller et al. [10] and decoded to the eight-channel loudspeaker arrangement using the AllRAD approach [11]. After application of the primary path transfer functions for the reference position, all spatialized innovation signals were normalized to produce a level of $70\,\mathrm{dB(A)}$ at the HATS. Subsequently, the spatialized signals at the HATS were generated from the normalized innovation signals for all measurement positions.

2.3 Evaluated ANC Systems

Fig. 3 illustrates the extension of the FxLMS algorithm into an FeLMS ANC system, as detailed in [3], for the evaluated setup. In an FxLMS system, the broadband disturbances $\mathbf{d}(n)$ at the HATS' microphones, modeled as the reference signals $\mathbf{x}(n)$ filtered by the respective primary paths $\mathbf{P}(z)$, are superimposed with the control signals $\mathbf{y}(n)$, resulting in the error signals $\mathbf{e}(n)$. With the control signals generated by filtering $\mathbf{x}(n)$ with a set of adaptive linear filters $\mathbf{W}(z)$ and applying the secondary paths $\mathbf{S}(z)$, the error signal at HATS microphone m can be expressed as

$$e_m(n) = d_m(n) + \sum_{i,j} \left(\mathbf{w}_{i,j}^T(n)\,\mathbf{x}_i(n)\right) * \mathbf{s}_{j,m}(n), \quad (1)$$

[1] `https://plugins.iem.at`

where $*$ indicates the convolution operation, $\mathbf{s}_{j,m}$ denotes the impulse response of $S_{j,m}(z)$ between secondary loudspeaker j and HATS microphone m, $\mathbf{x}_i(n) = [x_{i,0}(n), x_{i,1}(n), ..., x_{i,N-1}(n)]^T$ is the reference signal vector at primary loudspeaker i, and $\mathbf{w}_{i,j}(n) = [w_{i,j,0}(n), w_{i,j,1}(n), ..., w_{i,j,N-1}(n)]^T$ is the coefficient vector of $W_{i,j}(z)$, controlling the reference signal at primary loudspeaker i via secondary loudspeaker j, with filter order N at time n.

The filter coefficients are updated via the LMS algorithm, which takes the error signals $\mathbf{e}(n)$ and the filtered reference signals $\mathbf{r}(n)$ as inputs. Instead of the typical approach of filtering $\mathbf{x}(n)$ via an offline estimate of the secondary paths $\hat{\mathbf{S}}(z)$, in this simulation we can substitute $\hat{\mathbf{S}}(z)$ with our actual secondary paths $\mathbf{S}(z)$. The update equation for the filter coefficients $\mathbf{w}_{i,j}(n)$ is expressed as

$$\mathbf{w}_{i,j}(n+1) = \mathbf{w}_{i,j}(n) - \mu\, \mathbf{r}_{i,j}^T(n)\, \mathbf{e}(n), \qquad (2)$$

where $\mathbf{r}_{i,j} = [\mathbf{r}_{i,j,0}(n), \mathbf{r}_{i,j,1}(n), ..., \mathbf{r}_{i,j,N-1}(n)]^T$ denotes the filtered reference signal vectors for reference signal i, filtered with the secondary paths $\mathbf{S}_j(z)$ from secondary loudspeaker j to both HATS microphones, and μ is the adaptation step size.

In an FeLMS system both LMS input signals are additionally filtered with a weighting filter $H(z)$. Here, $H(z)$ denotes an A-weighting of the LMS input signals, implemented as a 7th order digital IIR filter derived via the improved matched z-transform method [12]. With $\mathbf{r_f}(n)$ and $\mathbf{e_f}(n)$ denoting the perceptually filtered versions of $\mathbf{r}(n)$ and $\mathbf{e}(n)$, Eqn. (2) becomes:

$$\mathbf{w}_{i,j}(n+1) = \mathbf{w}_{i,j}(n) - \mu\, \mathbf{r_f}^T_{i,j}(n)\, \mathbf{e_f}(n). \qquad (3)$$

To improve the convergence behavior of both ANC systems, the Normalized LMS (NLMS) algorithm [13] is employed, normalizing the adaptation step size by the time-smoothed total maximum energy over all $\mathbf{r}_{i,j}(n)$ and $\mathbf{r_f}_{\,i,j}(n)$, respectively.

As previous studies have shown, that the perceived spatial extent of ANC systems increases when limiting the control bandwidth [10], the evaluation of both FxNLMS and FeNLMS algorithms was conducted for both fullband and bandlimited ANC systems, i.e. at sample rates $f_{s,anc} = \{44.1\,\text{kHz}; 4410\,\text{Hz}\}$ with respective control filter lengths of 512 and 51 taps ($\hat{=}$ 12 ms).

2.4 Adaptation

The adaptation for all ANC systems, bandwidth conditions, and innovation signals was conducted for the reference position only. Step sizes for all conditions were set individually to ensure convergence after 70 s of the innovation signal.

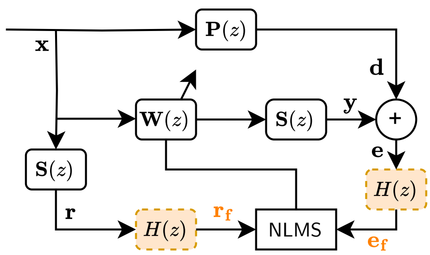

Figure 3. Extension of the FxNLMS algorithm into an FeNLMS system via added weighting filters $H(z)$ (orange) for the evaluated setup.

Fig. 4 shows the semitone-smoothed error power spectral densities (PSD) for the left HATS channel at the reference position both without ANC and after the adaptation process for all conditions. At the point of cancellation, substantial noise reduction is achieved by both FxNLMS and FeNLMS algorithms for white and pink noise in both bandwidth conditions. The FeNLMS PSDs show a bathtub-shaped frequency characteristic due to the applied A-weighting with a slight amplification of very low frequencies, while the FxNLMS algorithm tends to focus more on the reduction of higher frequency components. However, for driving noise, only the FeNLMS algorithm manages to achieve substantial noise reduction, while the FxNLMS algorithm only reduces very low frequency components and some harmonics caused by the car's combustion engine. The error PSDs for the bandlimited condition are in good agreement with the fullband condition up to just below the systems' Nyquist frequency at 2205 Hz, except for the FxNLMS algorithm for white noise, which achieves greater noise reduction in the controlled frequency range in the bandlimited condition.

3. EVALUATION

In order to evaluate the controlled sound field for rotations and transitions of the HATS extending from the sweet spot at the reference position, the control- and innovation signals were superimposed at all measurement positions. For each condition, the spatialized control signals were generated by filtering the normalized innovation signals with the respective converged adaptive filter and then applying the

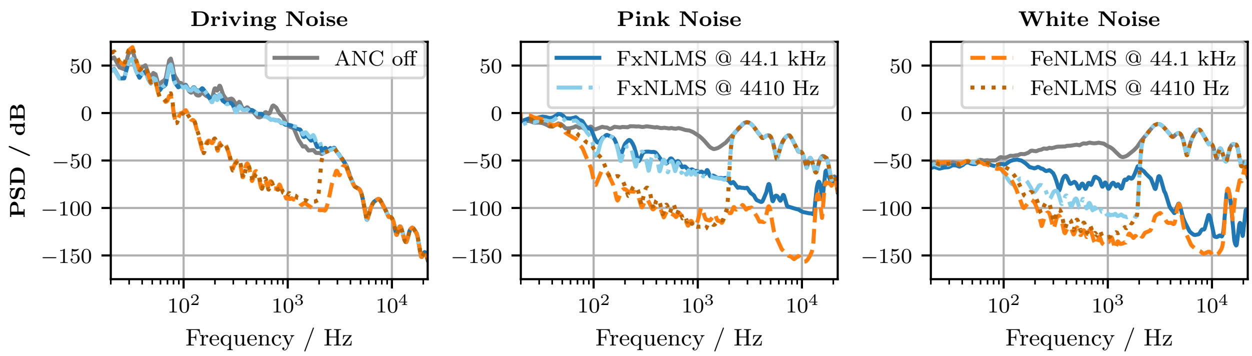

Figure 4. Error power spectral densities (PSD) at the reference position at left HATS channel for all control conditions after convergence. To prevent obscuring any data points, legend items are distributed among subplots.

corresponding secondary paths. The duration of the generated stimuli was 10 s. Afterwards, the following metrics were calculated in MATLAB R2024a at all measurement positions for both the uncontrolled spatialized innovation signals and all control conditions.

RMS. The monaural root mean square (RMS) value for the left HATS channel. Lower is better.

Loudness. The binaural loudness calculated using MATLAB's Audio Toolbox implementation of the Moore-Glasberg model [14] for signals captured at the eardrum. Lower is better.

Sharpness. The monaural acoustic sharpness of the left HATS channel computed using MATLAB's Audio Toolbox implementation of the model in DIN 45692 [15]. Lower is better.

PEMO-Q. The monaural Perceptual Similarity Measure (PSM) calculated by the PEMO-Q [2] [16] between the signal at the left HATS channel at the reference position and all other measurement positions. The PSM is calculated from the correlation between internal representations of level-normalized reference and test signals based on the Oldenburg Perception Model (PEMO). Higher is better.

MBSTOI. The reference-based Modified Binaural Short-Time Objective Intelligibility (MBSTOI) [3] [17] evaluated for a potential communication scenario, in which the adaptation of the ANC filters is paused, and the headrest loudspeakers are used to also play speech signals. To limit potential speaker-related biases the mean MBSTOI was calculated over the first sentence of each of the six speech samples provided in the EBU SQUAM material [4] in English, German, and French, uttered by male and female speakers. With the speech samples spatialized to the HATS using the secondary transfer paths and normalized to 55 dB(A), the MBSTOI was calculated from the speech samples in noise with the reference condition of speech samples spatialized to the HATS without any innovation signal present. Higher is better.

For monaural metrics, only signals at the left HATS channel were evaluated, because for rotations of the HATS greater fluctuations caused by the control signals can be expected at the ipsilateral ear, while for transitions to the front there is little difference between the channels due to the symmetric arrangement of the measurement setup.

4. RESULTS

The evaluated metrics for all ANC and innovation signal conditions are displayed in Fig. 5 for HATS rotations, and in Fig. 6 for transitions of the HATS. Prior to an in-depth discussion of the results, it is possible to discern several general trends from the data. For white noise there is little difference between algorithms, except for sharpness close to the reference position and coloration compared to the reference position expressed via the PEMO-Q values. For white and pink noise, and a translation of 2 cm to 5 cm, an interference effect is visible as the HATS exits the acoustic shadow provided by the headrest against the mid-to-back primary loudspeakers. For driving noise, there is virtually no difference per algorithm between bandwidth conditions due to the strong spectral tilt of the innovation signal. For

[2] https://uol.de/en/mediphysics/downloads/pemo-q
[3] http://ah-andersen.net/code/
[4] https://tech.ebu.ch/publications/sqamcd

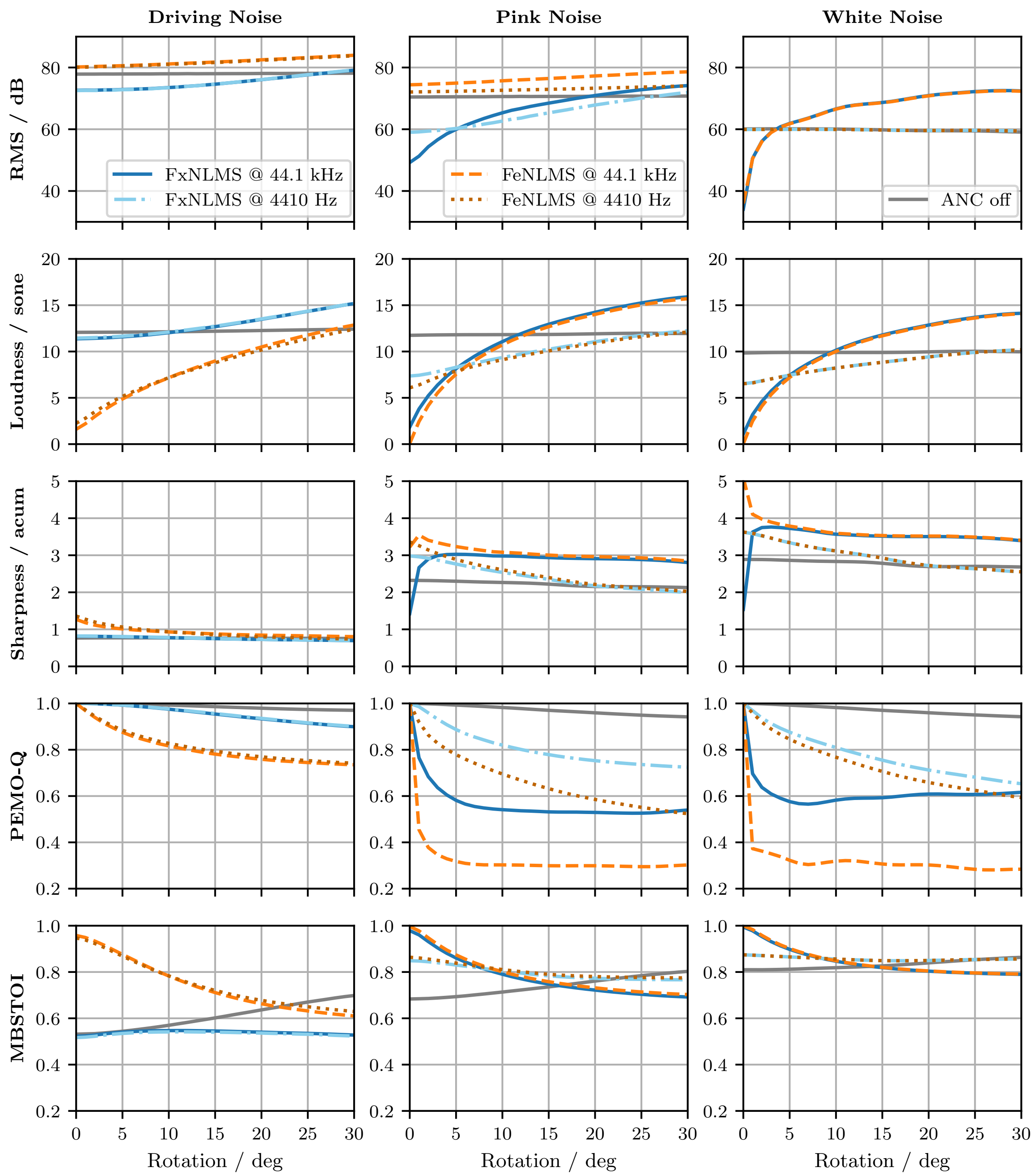

Figure 5. Evaluated metrics (rows) for all innovation signals (columns) as a function of HATS *rotation* from the reference position without ANC, and for fullband and bandlimited FxNLMS and FeNLMS ANC systems. To prevent obscuring any data points, legend items are distributed among subplots.

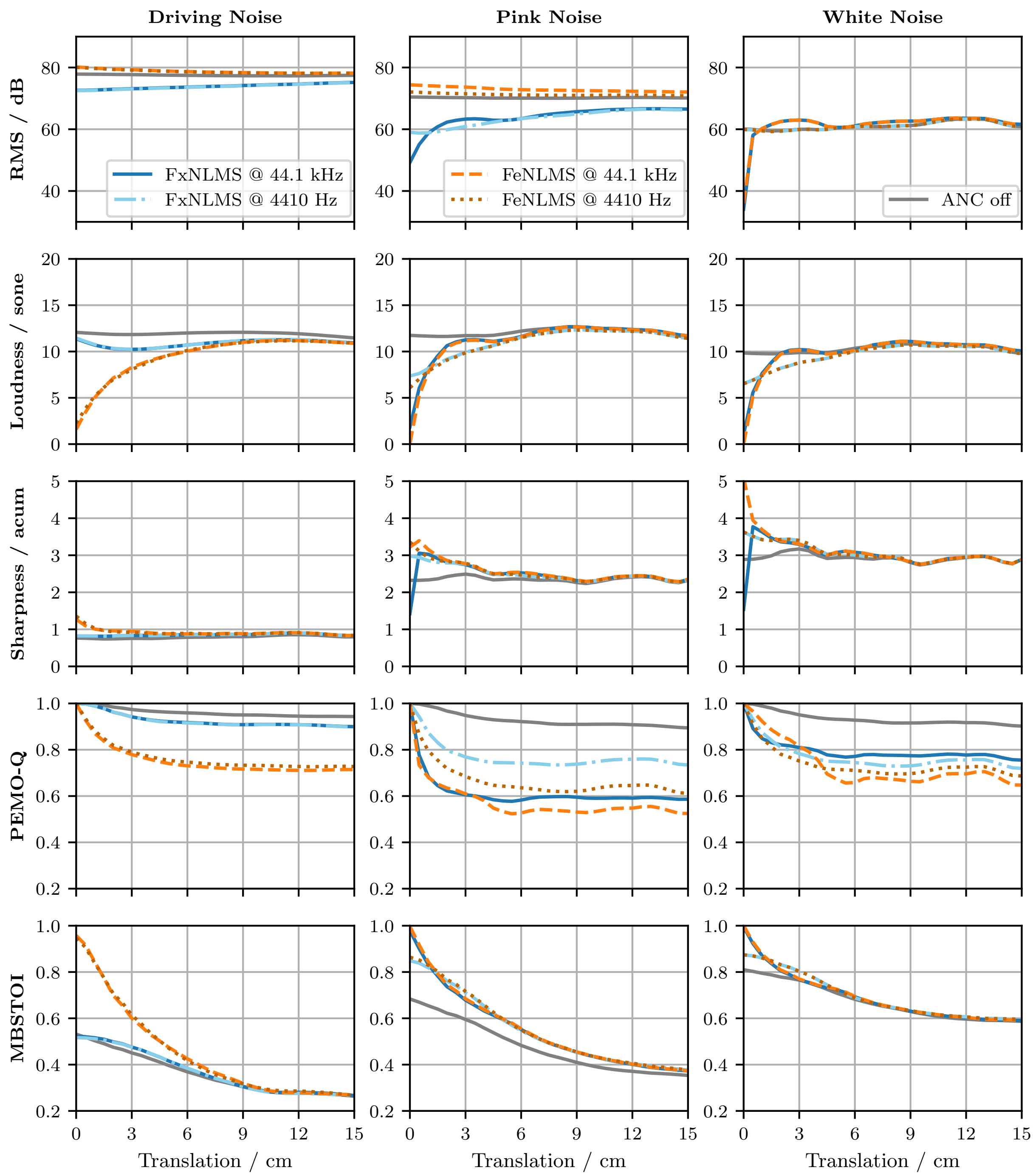

Figure 6. Evaluated metrics (rows) for all innovation signals (columns) as a function of HATS *translation* from the reference position without ANC, and for fullband and bandlimited FxNLMS and FeNLMS ANC systems. To prevent obscuring any data points, legend items are distributed among subplots.

the other innovation signals, compared to the fullband condition, the bandlimited condition generally results in smaller deviations from the data without ANC close to the reference position. The effects of the bandlimited condition also decrease more gradually with increasing rotation and translation from the reference position.

RMS. For white noise, both fullband ANC systems achieve a substantial reduction at the reference position but produce increased RMS values from 4° rotation and from $1\,\mathrm{cm}$ to $11\,\mathrm{cm}$ translation. The bandlimited ANC systems cause virtually no change in RMS. For pink noise, both FxNLMS systems manage a reduction in RMS that decreases for increasing rotation and translation, with the fullband condition performing better only near the reference position. Both FeNLMS systems cause an increase in RMS, that increases with rotation and slightly decreases with translation. For driving noise, these general trends between algorithms remain. While the FxNLMS systems achieve less reduction in RMS at the reference position compared to pink noise, the decrease in reduction for rotation and translation is more gradual.

Loudness. For white noise, similar trends are visible for the fullband condition as in the RMS results with the area of effect extending slightly further. Not visible in the RMS data, the bandlimited condition achieves some loudness reduction up to 25° rotation and $6\,\mathrm{cm}$ translation. Contrary to the RMS results, the FeNLMS algorithm achieves loudness reduction for both pink and driving noise, due to the focus on perceptually relevant frequency regions. While for pink noise, the FeNLMS systems achieve higher loudness reduction at the reference position, similar loudness reduction to the results for white noise is achieved for all conditions for head movements. For driving noise, the FeNLMS algorithm achieves a substantial loudness decrease at the reference position, while the FxNLMS algorithm barely reduces the loudness of the innovation signal. Loudness reduction extends up to 25° rotation and $10\,\mathrm{cm}$ translation for the FeNLMS systems, while loudness is increased by the FxNLMS systems from 10° rotation but remains stable across translation.

Sharpness. For white and pink noise, sharpness is reduced at the reference position by the fullband FxNLMS system but increased for all other ANC conditions. For rotations, sharpness remains increased over the condition without ANC for fullband control but reduces to the uncontrolled value for bandlimited control at 17° rotation. For transitions, sharpness reduces to match the value without ANC at $7\,\mathrm{cm}$ for all ANC conditions. For driving noise, sharpness is only slightly increased for the FeNLMS algorithm near the reference position.

PEMO-Q. Only slight changes are observed for all uncontrolled innovation signals. For all innovation signals, the sound field produced by the FeNLMS algorithm exhibits lower perceptual similarity to the reference position per bandwidth condition than that produced by the FxNLMS algorithm, with larger differences visible for rotation of the HATS. For fullband control, and white and pink noise, rotations of only 2° already cause a drop in perceptual similarity before values remain constant from 5°, indicating substantial coloration compared to the reference position, especially for the FeNLMS algorithm. An ongoing, more gradual decrease is visible for bandlimited conditions and driving noise. Across translations, the decline in perceptual similarity is less steep and values remain mostly constant from $5\,\mathrm{cm}$ translation for all conditions.

MBSTOI. Since the speech audio is played back via the headrest loudspeakers, intelligibility without ANC increases with rotation, because the ipsilateral ear moves towards the left loudspeaker. Similarly, intelligibility decreases with translation, because the HATS moves away from the loudspeakers. For white and pink noise, both fullband ANC systems enable perfect intelligibility at the reference position that decreases to levels observed without ANC by 12° rotation and $3\,\mathrm{cm}$ translation for white noise, and 15° rotation for pink noise. For larger rotation, intelligibility values fall below those of the uncontrolled condition. The bandlimited ANC systems cause slightly lower intelligibility at the reference position, but show a more gradual decline with increased rotation, extending the area of effect to 20°. Across translations, intelligibility is the same for all ANC systems from $5\,\mathrm{cm}$. For driving noise, only the FeNLMS algorithm causes a substantial increase in intelligibility with the effect extending to 20° rotation and $8\,\mathrm{cm}$ translation.

5. CONCLUSION

In a co-simulation of an active headrest system, a perceptually motivated FeNLMS algorithm using A-weighting was compared to an FxNLMS algorithm for fullband and bandlimited control with white, pink, and driving noise as innovation signals. Extending from the point of cancellation, the sound field produced by the ANC measures was evaluated for head rotations and transitions to the front based on RMS, binaural loudness, sharpness, PEMO-Q, and MBSTOI.

While the FeNLMS algorithm increases RMS values for pink and driving noise, the adaptation focus on perceptually relevant frequency regions causes a substantial reduction in loudness surrounding the point of cancellation.

For white and pink noise, there is only little difference between both algorithms in loudness and speech intelligibility, but the FeNLMS algorithm causes an increase in sharpness at the reference position and an increased coloration for head movements. However, for driving noise, the FeNLMS algorithm achieves vastly better loudness reduction and an increase in speech intelligibility.

While for white and pink noise, both algorithms perform better at the point of cancellation for the fullband condition when examining RMS, loudness, and MBSTOI, differences from the uncontrolled condition decrease more gradually for the bandlimited ANC systems. Further supported by the lower sharpness change and reduced coloration for head movements, an increased spatial extent is suggested for bandlimited control. For driving noise, the bandlimited ANC systems perform equally well as the fullband systems.

Future work will focus on the conduction of listening experiments to verify the simulation results.

6. REFERENCES

[1] S. Kuo and D. Morgan, "Active Noise Control: A Tutorial Review," *Proceedings of the IEEE*, vol. 87, no. 6, pp. 943–973, 1999.

[2] E. Zwicker and H. Fastl, *Psychoacoustics - Facts and Models*. Springer Berlin, Heidelberg, 2007.

[3] S. Kuo and J. Tsai, "Residual Noise Shaping Technique for Active Noise Control Systems," *J. Acoust. Soc. Am.*, vol. 95, no. 3, pp. 1665–1668, 1994.

[4] H. Bao and I. M. S. Panahi, "Using A-Weighting for Psychoacoustic Active Noise Control," in *Proc. of the 2009 Annual International Conference of the IEEE Engineering in Medicine and Biology Society*, (Minneapolis, USA), pp. 5701–5704, 2009.

[5] H. Bao and I. M. S. Panahi, "A Perceptually Motivated Active Noise Control Design and Its Psychoacoustic Analysis," *Etri Journal*, vol. 35, no. 5, pp. 859–868, 2013.

[6] P. R. Benois, U. Zölzer, and V. Papantoni, "Psychoacoustic Hybrid Active Noise Control Structure for Application in Headphones," in *Proc. of the 25th International Congress on Sound and Vibration*, (Hiroshima, Japan), 2018.

[7] C. Blöcher, A. Sontacchi, and T. Hatheier, "Impact of Perceptual Error Shaping in Active Noise Control Across Signals with Diverse Spectral Tilt," in *Fortschritte der Akustik - Proc. of DAS/DAGA 2025*, (Copenhagen, Denmark), 2025. Without peer review.

[8] P. Majdak, P. Balazs, and B. Laback, "Multiple Exponential Sweep Method for Fast Measurement of Head-Related Transfer Functions," *J. Audio Eng. Soc.*, vol. 55, pp. 623–637, 2007.

[9] S. Riedel, M. Frank, and F. Zotter, "The Effect of Temporal and Directional Density on Listener Envelopment," *J. Audio Eng. Soc.*, vol. 71, pp. 455–467, 2023.

[10] F. Holzmüller and A. Sontacchi, "Perceived Spatial Extent of Local Active Noise Control for Broadband Disturbances," in *Proc. of the AES 5th International Conference on Automotive Audio*, (Gothenburg, Sweden), 2024.

[11] F. Zotter and M. Frank, "All-Round Ambisonic Panning and Decoding," *J. Audio Eng. Soc.*, vol. 60, 2012.

[12] D. W. Gunness and O. S. Chauhan, "Optimizing the Magnitude Response of Matched Z-Transform Filters (MZTI) for Loudspeaker Equalization," in *Proc. of the AES 32nd International Conference*, (Hillerød, Denmark), 2007.

[13] D. Slock, "On the Convergence Behavior of the LMS and the Normalized LMS Algorithms," *IEEE Transactions on Signal Processing*, vol. 41, no. 9, pp. 2811–2825, 1993.

[14] B. C. J. Moore and B. R. Glasberg, "Modeling Binaural Loudness," *J. Acoust. Soc. Am.*, vol. 121, no. 3, pp. 1604–1612, 2007.

[15] DIN German Institute for Standardization, "DIN 45692 – Messtechnische Simulation der Hörempfindung Schärfe," 2009.

[16] R. Huber and B. Kollmeier, "PEMO-Q – A New Method for Objective Audio Quality Assessment Using a Model of Auditory Perception," *IEEE Transactions on Audio, Speech, and Language Processing*, vol. 14, no. 6, pp. 1902–1911, 2006.

[17] A. H. Andersen, J. M. de Haan, Z.-H. Tan, and J. Jensen, "Refinement and Validation of the Binaural Short Time Objective Intelligibility Measure for Spatially Dverse Conditions," *Speech Communication*, vol. 102, pp. 1–13, 2018.